Additive effects of basalt enhanced weathering and biochar co-application on carbon sequestration, soil nutrient status and plant performance in a mesocosm experiment

Nicolas Honvault, Marie-Laure Tiouchichine, Joana Sauze, Clément Piel, Damien Landais, Sébastien Devidal, Emmanuel Gritti, Delphine Bosch, Alexandru Milcu

Additive effects of basalt enhanced weathering and biochar co-application on carbon sequestration, soil nutrient status and plant performance in a mesocosm experiment

Nicolas Honvault [a,*], Marie-Laure Tiouchichine [a], Joana Sauze [a], Clément Piel [a], Damien Landais [a], Sébastien Devidal [a], Emmanuel Gritti [a], Delphine Bosch [b], Alexandru Milcu [a,c]

[a] Montpellier European Ecotron, Univ Montpellier, CNRS, Campus Baillarguet, 34980, Montferrier-sur-Lez, France
[b] Geosciences Montpellier, UMR-5243 CNRS, Université de Montpellier, 34095, Montpellier, France
[c] CEFE, Univ Montpellier, CNRS, EPHE, IRD, 34293, Montpellier, France

ARTICLE INFO

Editorial handling by Adrian Bath

Keywords:
Carbon sequestration
Basalt
Biochar
Enhanced weathering
Co-application
Negative emission technologies
Mesocosm
Soil nutrient availability

ABSTRACT

Co-deployment of a portfolio of carbon removal technologies is anticipated in order to remove several gigatons of carbon dioxide from the atmosphere and meet climate targets. However, co-application effects between carbon removal technologies have rarely been examined, despite multiple recent perspectives suggesting potential synergies between basalt enhanced weathering and biochar application. To study the co-application effects of basalt for enhanced weathering and biochar on carbon sequestration, along with related co-benefits and risks, we conducted a fully replicated factorial mesocosm experiment with wheat. Basalt applied alone (74 t ha^{-1}) resulted in an estimated carbon sequestration potential of 1.13 t of equivalent CO_2 ha^{-1} over the course of approximately 6 months. Co-application with biochar (12 t ha^{-1}) did not significantly increase estimated carbon sequestration potential. Total alkalinity fluxes and isotopic evidence indicated nearly exactly additive effects of basalt and biochar co-applied, with no significant interaction effect. Biochar carbon sequestration, approximately 32 t of equivalent CO_2 ha^{-1} in our experiment, was unaffected by basalt addition during our experiment. Co-benefits of basalt and biochar on plant biomass as well as nutrient uptake and availability similarly mostly showed additive tendencies when co-applied. Nonetheless, a few synergistic tendencies were observed when co-applied for plant potassium and magnesium uptake as well as soil calcium availability. Soil calcium availability increased by 126% compared to expected effects based on separate application. Finally, we did not observe a reduction in the increased uptake of potentially harmful trace elements released from basalt when co-applied with biochar. Overall, our results support the co-application of basalt for enhanced weathering and biochar, with additive effects on carbon sequestration and additive, if not synergistic, effects on associated co-benefits.

1. Introduction

To meet international climate targets, significant reductions in greenhouse gas (GHG) emissions are necessary, along with the development and large-scale deployment of carbon dioxide (CO_2) removal technologies (IPCC, 2022). A portfolio of technologies is anticipated to be required to address the challenge of removing several hundred gigatons (Gt) of CO_2 from the atmosphere (Amann and Hartmann, 2019). However, the co-deployment of technologies that share environmental compartments may impact their carbon (C) sequestration potential (Buss et al., 2021; Azeem et al., 2022). Consequently, recent perspectives highlight the urgent need to investigate interactions and plausible synergies among CO_2 removal technologies (Buss et al., 2021; Janssens et al., 2022; Hagens et al., 2023). In this context, the co-application of silicate rocks for enhanced weathering (EW) and biochar to soils have been suggested as a particularly promising approach for carbon dioxide removal with minimal competition with food production (Amann and Hartmann, 2019; Buss et al., 2021; Hagens et al., 2023).

EW is a geoengineering CO_2 removal technology that builds upon the natural process of silicate weathering, which is a key part of the Earth's carbon cycle that regulates the atmospheric CO_2 concentration over

geologic time scales (ten Berge et al., 2012). During silicate weathering, minerals react with carbonic acid formed from CO_2 dissolved in rainwater, which leads to the conversion ofCO_2 into bicarbonates and carbonates. Silicate dissolution thus results in increased total alkalinity, while simultaneously releasing base cations such as Ca^{2+}, Mg^{2+}, Na^{+} and K^{+} (Beerling et al., 2018; Hartmann et al., 2013). Carbonates may then either be transported to the ocean via run-off, or precipitate to form solid soil carbonates, with both processes resulting in stable carbon storage on timescales of $\sim 10^4$ years (Kelland et al., 2020; Larkin et al., 2022; Zamanian et al., 2016). EW involves accelerating this natural process by spreading finely ground silicate rocks to agricultural soils via increased rock surface area and moisture retention, both of which are favorable to weathering (Hartmann et al., 2013; Schuiling and Krijgsman, 2006). Enhanced weathering was proposed to potentially sequester up to 1–2 billon tons of CO_2–C per year by 2100 (Almaraz et al., 2022; Beerling et al., 2018). However, the carbon sequestration potential of EW is still sparsely studied, with documented conflicting estimates notably owing to different minerals (Beerling et al., 2020; Kantzas et al., 2022; Palandri and Kharaka, 2004; Vienne et al., 2022, 2023). Recent studies for basalt report a large range of C sequestration potentials, ranging from 73 to 13 kg of equivalent CO_2 t^{-1} rock $year^{-1}$ (or 2.4 to 0.43 t of equivalent CO_2 ha^{-1}) across various experimental durations (Kelland et al., 2020; Vienne et al., 2022, 2023; Reershemius et al., 2023).

Biochar, the carbon-rich residue from biomass pyrolysis, can store organic C in soils for hundreds to thousands of years (Lehmann et al., 2015) and is another important CO_2 removal technology sequestrating atmospheric CO_2 captured by plants. The long residence time of biochar in soil is attributed to its interactions with soil minerals and its lower susceptibility to microbial degradation compared to other C sources due to its aromatic nature, among other factors (Lehmann et al., 2015; Wang et al., 2016). Global biochar C sequestration potential is estimated at approximately 1–1.8 billion tons CO_2–C per year (Woolf et al., 2010; Paustian et al., 2016; Smith 2016). In addition to C sequestration, biochar also tends to increase soil cation exchange capacity (Hossain et al., 2010; Laird et al., 2010; Zhang et al., 2021), nutrient availability (Wang et al., 2014; Ding et al., 2016; Zhang et al., 2021), soil microbial activity (Palansooriya et al., 2019; Pokharel et al., 2020) and soil water holding capacity (Ding et al., 2016; Jeffery et al., 2011; Wei et al., 2023) among other co-benefits for soil quality and fertility (Dai et al., 2020; Ding et al., 2016; Jeffery et al., 2011).

Several recent perspectives postulated the existence of synergistic effects when biochar is co-applied with EW, further improving C sequestration potential (Buss et al., 2021; Janssens et al., 2022; Hagens et al., 2023). When co-applied with basalt, biochar's influence on soil properties may indeed enhance basalt dissolution rates, thus maximizing their cumulative C sequestration potential (Amann and Hartmann 2019; Azeem et al., 2022). Indeed, biochar can influence soil microbial communities and tend to increase their activity (Palansooriya et al., 2019; Pokharel et al., 2020; Ren et al., 2021). Rock weathering can be significantly mediated by microorganisms (Hoffland et al., 2004; Uroz et al., 2009; Azeem et al., 2022), suggesting that change in microbial activity due to biochar may improve basalt dissolution (Vicca et al., 2022). In addition, biochar application can potentially act as a sink for products of basalt dissolution such as cations or silicon (Wang et al., 2018), directly via increased soil cation exchange capacity (CEC) or indirectly via improved plant growth and nutrient uptake (Ding et al., 2016; Laird et al., 2010; Xiang et al., 2017). Lower soil availability of products of basalt dissolution would then be expected to increase dissolution rates. Given that limited water availability may largely reduce C sequestration potential (Cipolla et al., 2022; Reynaert et al., 2023), enhanced soil water holding capacity via biochar addition may also contribute to improved EW efficiency (Buss et al., 2021). In addition, reduced GHG emission rates (especially of N_2O and CO_2) have also been reported for both (Kantola et al., 2023; Vienne et al., 2023), thus potentially maximizing the system's C sequestration potential when co-applied. However, synergies between EW and biochar application for C sequestration have been suggested based on literature reviews (Amann and Hartmann, 2019; Buss et al., 2021; Smith, 2016), while experimental evidence is still lacking.

Besides potential synergistic effects on C sequestration, biochar and EW have also demonstrated concurrent effects on soil fertility suggesting complementary effects between both technologies for plant growth. Indeed, basalt EW releases plant essential nutrient such as K, P, Ca, Mg, Fe and Mn (Beerling et al., 2018; Kantola et al., 2017; Vienne et al., 2022), tends to increase soil quality (pH, CEC, etc.) (Anda et al., 2013; Swoboda et al., 2022) and was observed to reduce N losses (Swoboda et al., 2022). Recent results suggest increases in Mg availability between 100 and 800% (Amann et al., 2020; Kelland et al., 2020; ten Berge et al., 2012; Vienne et al., 2022), increases in K availability between 1 and 10% (Renforth et al., 2015; Swoboda et al., 2022), improvements in soil cation exchange capacity by 20–87% (Anda et al., 2013; Gillman et al., 2002) or reduced nitrogen leaching by up to 55% in soils amended with crushed silicate rocks (Amann et al., 2020). Basalt EW may also protect crops against pests and diseases (Luyckx et al., 2017), notably through improved Si availability and uptake (+50–180%) (ten Berge et al., 2012). Biochar similarly tends to increase pH (Laird et al., 2010; Wang et al., 2014; Zhang et al., 2021), improve CEC by up to 4–40% (Hossain et al., 2010; Laird et al., 2010; Zhang et al., 2021) and improve porosity by up to 20% (Lu et al., 2014), all of which can potentially contribute to improve soil fertility. Biochar also tends to improve plant nutrient uptake, via increased nutrient availability, for instance +60–670% for K, Ca, Na and Mg availability in Wang et al. (2014), but also improved root development such as + 39% root area in a meta-analysis by Xiang et al. (2017). Coupled with basalt EW, biochar co-application may thus lead to complementary fertilisation and improved plant nutrient use efficiency when co-applied (Buss et al., 2021). In addition, EW negative side effects via trace metal release (*e.g.*, Ni and Cr) from EW may be reduced via adsorption of trace elements on biochar. Important reduction in trace element uptake after biochar addition have been reported, for instance by 44% in Natasha et al. (2022). Although basalt EW is expected to have lower risks of trace element contamination due to inherently lower contents relative to other ultramafic rocks, potential effects still need to be examined and minimized to ensure environmental safety (Vienne et al., 2022).

To experimentally investigate the potential synergistic and additive effects of co-deploying basalt EW and biochar for soil carbon sequestration, as well as their associated co-benefits for soil fertility and plant growth, we conducted a mesocosm experiment under controlled conditions, with winter wheat (*Triticum aestivum* L.) as a model crop. The amendments consisted of basalt (74 t ha^{-1}) and biochar (12 t ha^{-1}), both individually and in combination, a fully replicated factorial design that allowed to examine potential interactions. To the best of our knowledge, this study represents one of the first effort to investigate the co-application of these two CO_2 removal technologies in a mesocosm setting. We hypothesized that the combined application of basalt and biochar would result in synergistic or at least additive effects on: (1) soil carbon sequestration, as evidenced by changes in soil carbon pools, alkalinity release based on element budget in plants, soil and leachate pools, and shifts in an isotopic proxy of basalt dissolution; (2) the availability of soil nutrients, including P, K, Mg, Ca and (3) plant performance, characterized by biomass, nutrient uptake and availability. Additionally, we also hypothesized that (4) the combined application of basalt and biochar would result in reduced availability and plant uptake of Ni and Cr.

2. Material and methods

2.1. Experimental setup

The mesocosm experiment was conducted in the Macrocosms experimental platform of the Montpellier European Ecotron (France,

43°68′ N, 3°87’ E). The Macrocosms units consist of 30 m^3 transparent domes which are covered by a material that is highly transparent to light and UV radiation (a 250 μm thick Teflon-FEP film from DuPont, USA). Within each dome, the main abiotic characteristics—air temperature, humidity, and CO_2 concentration—of the atmospheric compartment of the domes are controlled. The design consisted of application of biochar (12 t ha^{-1}), basalt (74 t ha^{-1}) separately or co-applied as well as a control without any amendments, leading to four treatment combinations. Moderate biochar and basalt application rates were selected based on literature to examine more agronomically realistic practices (Joseph et al., 2021). Each combination was replicated six times, resulting in a total of twenty-four mesocosms. The mesocosms were organized into two blocks of twelve. Every procedure, including watering, leachate collection and measurements was staggered by a one-day interval between the two blocks. Blocks were further split between two Macrocosm domes (Roy et al., 2021) with treatments per block evenly split between Macrocosm domes. Within a dome, mesocosms locations were randomized weekly per block. This strategy was implemented to ensure minimal experimental deviation between blocks and to address technical limitations during measurements.

The mesocosms (approx. 600 × 400 × 350 mm) were designed to allow the establishment of two sections, an uncultivated area of approx. 300 × 300 mm to be used for gas exchanges measurements and a cultivated area encompassing all the remaining soil surface (Fig. 1). To allow for leachate collection, each mesocosm was outfitted with a 6 mm hole at its base, which was fitted with a collection valve. Leachate drainage and collection were further facilitated via an approximately 20 mm deep layer of neutral plastic beads (polypropylene) at the bottom of each mesocosm. To avoid soil export and possible clogging, a small plastic mesh (2.5 mm) protected the mesocosm outlet. Leachates were collected periodically as detailed in the irrigation and leachate collection section and were systematically measured.

2.2. Basalt and biochar characteristics

The basalt used was provided by Lava Union (Lava-Union, GmbH Kölner Str. 22, 53489 Sinzig, Germany). The micronized basalt powder (80% < 63 μm) originates from a German quarry in Rhineland-Palatinate near Koblenz. This basalt dust was selected based on its mineralogy and composition, especially its high pyroxene and plagioclase content (Table 1). Basalt powder’s specific surface area (20 $m^2\ g^{-1}$) was determined based on the BET method with N_2 (Brunauer et al., 1938). The biochar was produced from wood biomass and was selected for its physiochemical properties, particularly its high H:C ratio and specific surface area (Table 2). High biochar hydrogen to organic ratio, notably indicative of biochar carbon structure was selected to ensure high biochar stability and residence time (Lehmann et al., 2015).

Table 1
Basalt mineralogy, surface area and composition.

Basalt mineralogy		($g\ g^{-1}$)
Augite, aluminian	Magnesium Calcium Aluminum Iron Silicate	48
Anorthite, sodian, disordered	Sodium Calcium Aluminum Silicate	18
Monalbite	Sodium Aluminum Silicate	18
Forsterite ferroan	Magnesium Iron Silicate	7
Nepheline (Na-exchanged)	Sodium Aluminum Silicate	5
Magnetite	Iron Oxide	4
Specific surface area	20	$m^2\ g^{-1}$
Basalt composition		%
Si	SiO2	43.39
Mg	MgO	13.06
Fe	Fe2O3	12.58
Al	Al2O3	11.78
Ca	CaO	10.71
Na	Na2O	2.54
Ti	TiO2	2.08
K	K2O	0.96
P	P2O5	0.66
Mn	MnO	0.15
Sr	SrO	0.11
Cl	Cl	0.10
Cr	Cr2O3	0.09
S	SO3	0.06
Ni	NiO	0.06

Basalt mineralogy as determined via XRD, composition as determined by XRF and specific surface area as determined by BET method with N_2. Element expressed in total oxides.

Biochar was graciously provided by Hans Peter Schmidt (Ithaka Institute, Switzerland).

2.3. Soil preparation and growth conditions

The slightly acidic soil (pH_{H2O} = 6.0) used in the experiment is a Cambisol collected from a natural meadow at the Centre de Recherche en Ecologie Expérimentale et Prédictive—CEREEP ecotron IDF (CEREEP, France) (0–300 mm). Soil physicochemical properties are presented in Table 3. The soil was roughly sieved (20 mm) to remove large stones and root fragments. The mesocosms were filled three weeks before the beginning of the experiment, and the soil was rehydrated to 80% of its water holding capacity (WHC). An equivalent of 40 kg N ha^{-1} was added as ammonium nitrate during the first watering of the soil. At the start of the experiment (day 0, 29/08/22 and 30/08/22), wood biochar and basalt were applied at a rate of 12 t ha^{-1} and 74 t ha^{-1}, respectively, for the biochar only and basalt only conditions. The same rates were employed when applied alone as when biochar and basalt

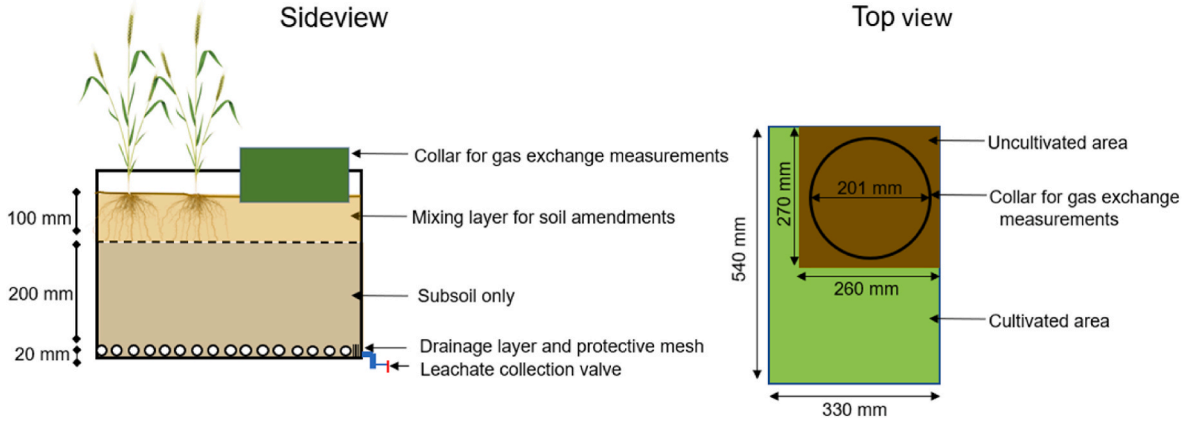

Fig. 1. Schematic diagrams showing side and top views of the mesocosm.

Table 2
Biochar physiochemical properties.

Density (kg m^{-3})[a]	320
Specific surface area (m^2 kg^{-1})[b]	189
Corrected density (g cm^{-3})[b]	1.5
Ash (550 °C) (%)[c]	8.3
pH_{CaCl2}[d]	8.5
Conductivity (µS cm^{-1})[e]	501
O_{tot} (%)[f]	5.9
N_{tot} (%)[g]	0.59
C_{tot} (%)[g]	85.1
TIC (%)[h]	0.7
H/C_{org}	0.3
O/C	0.053
C/N	143
P (%)[i]	0.1
Mg (%)[i]	0.2
Ca (%)[i]	1.6
K (%)[i]	0.5
Si (%)[i]	0.7
S (%)[i]	0.7
Ni (mg kg^{-1})[j]	4
Cr (mg kg^{-1})[j]	6

[a] DIN 51705: 2001-06.
[b] ISO 9277.
[c] DIN 51726.
[d] DIN ISO 10390.
[e] BGK III, C2: 2006-09, analog DIN ISO 11265.
[f] DIN 51733.
[g] DIN 51733.
[h] DIN 51726.
[i] DIN EN ISO 11885.
[j] DIN EN ISO 17294-2.

Table 3
Soil physiochemical properties.

Clay (%)	10.5
Silt (%)	19.2
Sand (%)	70.2
Corg (g kg^{-1})	11.1
Total N (%)	0.1
CEC (cmolc kg^{-1})	4.4
pH KCl	5.2
Exchangeable P (mg kg^{-1})	22.0
Exchangeable K (mg kg^{-1})	113.3
Exchangeable Mg (mg kg^{-1})	60.0
Exchangeable Ca (mg kg^{-1})	776.7

Corg: organic carbon concentration determined by dry combustion on decarbonated soil NF ISO 14235; Total N: total soil nitrogen as determined by Dumas method; CEC: CEC Metson NFX 31–130; Exchangeable cations determined via extraction with ammonium-acetate-EDTA buffer (Lakanen and Erviö, 1971) and determination through ICP-MS.

were co-applied. To allow for proper mixing of the amendments with the soil, the topsoil (0–100 mm) was removed from the mesocosms and separately thoroughly manually mixed with the amendments. This was also performed for the control condition without any amendment. After collecting sub-samples for initial characterization, the soil was returned to the mesocosms and adjusted to an approximate density of 1.3 kg per liter (kg L^{-1}). It was then watered to reach 80% WHC. Prior to sowing, the seeds of an early variety of winter wheat ("Filon" variety, Florimond Desprez, France) were pre-germinated on filter paper imbibed with distilled water in the dark at 6 °C for four days. The seedlings were then transplanted with 50 mm between plants per row and 80 mm between rows. Initial densities were doubled and then adjusted to the desired density (240 ind m^{-2}) two weeks after sowing. Environmental conditions were established at 26 °C with 60% relative humidity (RH) during the day and 16 °C with 70% RH at night. An exception was a vernalization period of three weeks, maintained at 8 °C with 70% RH during the day and 6 °C with 80% RH at night, which was applied to stimulate the development of reproductive organs. Macrocosm domes were employed as greenhouses, with natural daylight.

2.4. Irrigation and leachate collection

Mesocosms were irrigated bi-weekly for the first month and then weekly to maintain soil water content between 80 and 60% of bare soil WHC. For the first 3 months all mesocosms were watered with the same amount of deionised water regardless of the treatment. The amount was determined based on the average mesocosm weight of the driest treatment and was calculated to reach 80% of WHC for this treatment. The same amount of water was applied to both experimental blocks. After three months, owing to observed differences in evapotranspiration and decreased drainage frequency in our non-free draining mesocosms, each mesocosm was individually watered to achieve 80% WHC. This approach was adopted to minimize unsetting variations between treatments. Irrigation rates, cumulative irrigation and estimated evapotranspiration amounts are presented in Appendix A, B. Leachates were collected after 2, 4, 8, 12, and 24 weeks following the initiation of the experiment. During each collection, the mesocosms were watered approx. 24 h before leachate collection to reach 100% WHC. To guarantee an adequate volume for leachate analysis, the amount was increased by adding 0.26 L on top of the quantity equivalent to one day's evapotranspiration (0.2 L required for analysis, evapotranspiration tendencies calculated based on prior two weeks). Upon collection, mesocosms were inclined toward the collection valve and left to drain via polyethylene pipes connected to plastic bottles for approx. 24 h. Leachate volume was measured, and leachates were filtered at 0.45 µm and then acidified to pH 3 with trace-metal grade HNO_3 and stored in a fridge (6–10 °C) until analysis.

2.5. Soil CO_2, CH_4 and N_2O fluxes

A plastic PCV collar was permanently inserted at a depth of 40 mm in the uncultivated area, to act as base for the automatic chambers used for gas exchanges measurements coupled with an infrared analyser (LI-8100A; LI-COR Biosciences, Lincoln, NE, USA) with a cavity ring-down spectrometer (Picarro G2508; Picarro Inc., Santa Clara, CA, USA). The bare ground inside the plastic collar was filled with a shallow layer of neutral plastic beads (<10 mm, polypropylene) to avoid moss development and possible interferences for gas exchange measurements. Soil gas exchange measurements of CO_2, CH_4 and N_2O were performed twice a week for the first two weeks after experiment launch and then on a weekly basis. Automated measurements were carried out with twelve soil flux chambers (LI-COR 8100-104 Opaque Long-Term Chamber) connected to the control multiplexer (Li-8150; LI-COR Biosciences, Lincoln, NE, USA) and installed on permanent PVC collars. Measurements were 7 min and 30 s long with a 45-s pre-purge and a 45-s post-purge. Soil fluxes were computed using SoilFluxPro Software (v4.2; LI-COR Biosciences, Lincoln, NE, USA). N_2O, CO_2 and CH_4 fluxes were calculated from the G2508 raw data. Fluxes were derived from a linear model applied to 120 s of raw data for N_2O/CH_4 and 60 s for CO_2 and validated based on R-squared fits ($R^2 > 0.7$).

2.6. Plant, soil and leachate analysis

2.6.1. Plant

Wheat was harvested after approx. 6 months (176 days), specifically during the heading development stage, in order to also capture effects on root biomass and traits (Ghimire et al., 2020). Upon harvest, wheat was separated into seed, shoot and root biomass. Roots were carefully washed with deionised water to remove any remaining soil particles. A composite sample was used to determine root nutrient content. While immersed in deionised water, roots obtained from 200 cm^3 cylinder samplings were scanned with a STD4800 Calibrated Color Optical

scanner with special lighting system (S/N URUW009925-6714112, Optical Resolution 4800 dpi, max scan area: 22 × 30 cm). Root traits were then determined with the WinRHIZO software (Regent Instruments Inc., Quebec, Canada).

All biomass was dried for 48H at 60 °C. Biomass subsamples were milled and analyzed for total N (Dumas method) and C (dry combustion, CHNS Flash, 2000 Thermo Fisher Scientific) contents and macro-element concentration *i.e.* P, Ca, Mg, K, Na by dry combustion followed by ICP analysis (NF EN ISO 16634-1). Ni and Cr concentrations were determined for shoot and seed biomass after digestion with nitric and perchloric acid via ICP analysis (ISO 22036). Finally, seed and shoot Sr concentration and $^{87}Sr/^{86}Sr$ isotopic ratio was determined following calcination, digestion with extra pure nitric acid followed by ICP analysis. Samples for $^{87}Sr/^{86}Sr$ isotopic ratio determination were examined as detailed in part 2.9.

2.6.2. Soil sampling and analyses

Soil samples were collected at the start of the experiment and at harvest. At harvest, two types of soil composites were collected: topsoil from a depth of 0–100 mm, and subsoil from a depth of 100–300 mm. Every soil sample was analyzed for exchangeable P, K, Mg and Ca (Lakanen and Erviö, 1971); pH_{KCl} (NF ISO 10390); pH_{H2O} (AFNOR, 2012); N_{tot} (NF ISO 13878); CEC_{met} (ISO 23470); TC; N–NO3 and N–NH4 (ISO 14256); and exchangeable Sr (Kelland et al., 2020). Soil samples were air dried before exchangeable P, K, Mg, Ca, pH_{KCl}, pH_{H2O}, C_{org}, N_{tot}, CEC_{met} and Sr measurements. Soil samples for TC, N–NO_3, N–NH_4 were frozen at −20 °C before analysis. Exchangeable P, K, Mg, Ca were extracted with 0.5 N ammonium 0.02 M EDTA pH 4.65 followed by molybdenum blue colorimetry and atomic absorption spectroscopy (Lakanen and Erviö, 1971). Exchangeable Sr was extracted with 1 M NH_4CL adjusted to pH = 8 with a 1:20 soil:solution ratio for 20H (Kelland et al., 2020). Soil cation $^{87}Sr/^{86}Sr$ isotopic ratios were measured based on NH_4Cl extracts (Kelland et al., 2020) and as detailed in part 2.9. Soil N–NO_3 and N–NH_4 content were extracted with KCl 1 M and determined calorimetrically (ISO 142–562). Available nutrient stocks per soil layer (0–100 mm and 100–300 mm) were calculated based on density, depth and nutrient concentration and then summed to obtain a total stock value per mesocosm.

2.7. Leachate analysis

Leachates were analyzed for total Ca, Mg, P, K, Ni and Cr. For total Ca, Mg, P, K, Ni, Cr and Sr as well as $^{87}Sr/^{86}Sr$ isotopic ratio, 50 mL of the acidified samples were first evaporated, before adding ultrapure HNO_3 1 M. Samples for total Ca, Mg, P, K, Ni, Cr and Sr determination were then transferred in 2% HNO_3 for determination via ICP-OES (iCAP 7400, Thermo Fisher Scientific) or ICP-MS (Agilent 7700x) at Montpellier University using the AETE-ISO platform facilities.

2.8. Assessment of the carbon sequestration potential

Due to well-known challenges in directly measuring C sequestration rate in short-term weathering experiments (Kelland et al., 2020; Larkin et al., 2022; Reynaert et al., 2023; Vienne et al., 2022), the C sequestration potential was estimated via several complementary approaches. Total soil carbon content was measured with a CHN analyser (CHN Flash Smart AE, 2000 Thermo Fisher Scientific). Total soil carbonates were determined via CO_2 emission after addition of ortho-phosphoric acid in a heated reactor (180 °C) (NF EN 15936). The stocks of soil C and carbonates were calculated using the same method as applied to estimate the nutrient stocks. Two proxies of basalt dissolution were also employed: a cation release-based proxy and a Sr isotopy-based proxy, as detailed in section 2.9. The impact of basalt dissolution on the cation stocks (K, Mg, and Ca) in various pools — soil, leachates, and plant root, shoot, and seed biomass — was expressed as the difference from the control. The release rate of elements from added basalt was then calculated by normalizing for basalt surface area and dividing by experiment duration (see example for Mg in equation 1) (Kelland et al., 2020; Vienne et al., 2022):

$$\text{Eq.1}\quad Q_{Mg_{BAS}} = \frac{P_{BAS} + L_{BAS} + S_{BAS} - (P_{CONT} + L_{CONT} + S_{CONT})}{SA_{BAS} \times S}$$

where, Q_{MgBAS} = Mg release rate in mol m^{-2} SA_R s^{-1}, P_{BAS} = amount of Mg recovered in plants roots, shoots and seeds for basalt amended mesocosms (mol $mesocosm^{-1}$), L_{BAS} = amount of Mg recovered in leachates for basalt amended mesocosms (mol $mesocosm^{-1}$), S_{BAS} = amount of Mg recovered in soil extracts, exchangeable for basalt amended mesocosms (mol $mesocosm^{-1}$); P_{CONT} = amount of Mg recovered in plants roots, shoots and seeds for control mesocosms (mol $mesocosm^{-1}$), L_{CONT} = amount of Mg recovered in leachates for control mesocosms (mol $mesocosm^{-1}$), S_{CONT} = amount of Mg recovered in soil extracts, exchangeable for control mesocosms (mol $mesocosm^{-1}$); SA_{BAS} = Basalt surface area applied per surface: m^2 g^{-1} basalt x basalt application rate g m^{-2}; S = Second since experiment start.

Total release of major cations (K, Mg and Ca) was used as a proxy to calculate the total alkalinity release (Buckingham et al., 2022; Kantola et al., 2023; Vienne et al., 2023). Formation of secondary products and precipitates, no longer extracted from the soil exchangeable pools, are not accounted for in this estimation, providing a minimal estimate (Vienne et al., 2023). Inorganic carbon sequestration potential (t of equivalent CO_2 ha^{-1}) over the experiment duration was then calculated assuming η = 0.75 mol of CO_2 stored per mole of alkalinity release (Renforth, 2019). Inorganic carbon sequestration potential per year (t of equivalent CO_2 t $rock^{-1}$ $year^{-1}$) was linearly extrapolated (Vienne et al., 2023). Owing to the complex dynamics of alkalinity once it is released into soils and groundwater, the molar ratio of CO_2 sequestered per mole of alkalinity released (η) remains uncertain, with most studies employing a value for η between 0.5 and 1 (Amann et al., 2020; Kantola et al., 2023; Reynaert et al., 2023; Vienne et al., 2022, 2023). For the purpose of comparison, alternative estimates of inorganic carbon sequestration potential for η = 1 and η = 0.5 are presented in appendix C. Inclusion of plant cation uptake in estimated total alkalinity release rate is also subject to debate according to the fate of plant matter (Dietzen and Rosing, 2023). Thus, more conservative estimates excluding plant cation uptake are also presented in appendix C.

2.9. Sr radiogenic isotopes

Sr was used as a tracer of basalt weathering based on different $^{87}Sr/^{86}Sr$ isotopic ratio in the basalt and soil background (Kelland et al., 2020). Sr input in the distillated water used for watering is considered negligible (as observed in controls). Sr isotope analyses were performed in the ISOTOP-MTP laboratory (CNRS-University of Montpellier). For basalt Sr isotope analyses, two types of samples were analyzed: (i) total dissolution of basaltic powder without leaching, and (ii) analysis on leachate and residue obtained after leaching in 6 M HCl for 1 h at 95 °C and rinsing thrice with Milli-Q water (see Bosch et al. (2014) for details of the leaching procedure). Basalt powder and residue obtained after leaching were dissolved on a hot plate at 140 °C for 72 h using a mixture of concentrated HF and HNO_3 and addition of a few drops of $HClO_4$. After drying, concentrated HNO_3 was added to the residue and kept at 110 °C for 48 h, after which the solution was evaporated to dryness. Sr was chemically separated using two successive concentration/purification steps. Sr isotopes were analyzed using a Thermo-Fisher® Neptune Plus multi-collector (MC)-ICP-MS at the AETE-ISO platform facilities (Montpellier University). Standards were analyzed for each of the five unknowns in the bracketing mode. The average standard values were $^{87}Sr/^{86}Sr$ = 0.710253 ± 0.000008 (2σ) (n = 20) for the NBS987 Sr reference material. Matrices matching certified reference materials (BEN, basalt powder) were prepared and analyzed along with the samples and yielded the following results: $^{87}Sr/^{86}Sr$ = 0.703291 ±

0.000002 (2σ) (n = 2). Blank levels measured during analyses were of 44 pg for Sr and considered to be negligible for the studied samples.

As Ca doesn't fractionate from Sr during dilution, the amount of Ca derived from basalt weathering in plants and soils was calculated based on $^{87}Sr/^{86}Sr$ isotopic ratios and Sr:Ca concentrations ratios in basalt and soil (Capo et al., 1998) (equation 2). Since no notable divergence in Sr plant and soil isotopic ratios were observed in the biochar only addition (see results part 3.3), for the biochar and basalt combination the two-source mixing model was applied with the assumption that the isotopic ratios of basalt and initial soil could be employed to calculate the Ca derived from basalt, assuming a negligible contribution of biochar. Calculated amounts of Ca derived from basalt weathering in plants and soils were then multiplied by total Ca amount per pool to produce an alternative isotopic estimate of Ca release rate. Isotopic estimates of Ca release rates were then used to derive a second estimate of total alkalinity release and C sequestration via alkalinity release as presented in part 2.8. Leachate Ca fluxes were excluded from this estimate as leachates' $^{87}Sr/^{86}Sr$ isotopic ratio was only measured for the leachates collected after 169 days. However, Ca fluxes in leachates represented only between 2 and 3% of the total Ca fluxes (for all amendments, fluxes in plant, soil available pools and leachates).

Eq.2 $$F_{Ca=}\frac{(\delta_X-\delta_{Soil})K2}{(\delta_{basalt}-\delta_{soil})K2+(\delta_{basalt}-\delta_X)K1}$$

where F_{Ca} = fraction of Ca derived from basalt in a given pool; δ_X = $^{87}Sr/^{86}Sr$ isotopic ratio in the pool (plant or soil); δ_{Soil} = $^{87}Sr/^{86}Sr$ isotopic ratio in the control pool (soil) and δ_{basalt} = $^{87}Sr/^{86}Sr$ isotopic ratio in the basalt; K1=Sr:Ca ratio of basalt; K2=Sr:Ca ratio of soil.

2.10. Data analysis

All analyses were performed in R version 4.2.2 (R Core Team, 2022). Comparison at harvest for plant, soil and cumulative leached nutrients as well as other soil properties and cumulative GHG emission were performed via ANOVAs or Kruskal Wallis tests if ANOVA assumptions were not met. Planned comparison were performed with t-tests or Wilcoxon Mann Whitney tests if ANOVA assumptions were not met. Experimental block and dome effects were examined and later excluded based on no significant block and dome effect and better fit (based on R^2) when excluding block and dome effects. Differences in GHG rates were analyzed via linear mixed models incorporating blocks (2 blocks of 12 mesocosms each) treatment, time since experiment start, soil humidity and air temperature as explanatory variables and a random effect per time per mesocosm due to repeated measurement (package nlme V31). Minimal adequate models were selected based on Akaike Information Criterion (AIC). For mass balance calculations (cation budgets), uncertainty was propagated between pools (plant, soil and leachates) and corrected for subtraction of mean measurement of the control treatment by quadratic addition of the standard error (Kirchner, 2001). In order to investigate the interactions between biochar and basalt application alone or in combination, an interaction model (ANOVA) was produced with basalt application, biochar application and their interaction (basalt*biochar) as factors and element release rates and total alkalinity release rate as dependent variables. Co-application effects were also calculated as the effects when co-applied to the sum of effects alone (equation 3). Values over 100% indicate a synergistic effect, while values below 100% a less-than-additive effect.

Eq.3 $$Co-application\ effect_{Mg}=\frac{Mg_{biochar+basalt}}{Mg_{basalt}+Mg_{biochar}}$$

3. Results

3.1. Inorganic carbon sequestration potential via alkalinity release

The total soil stocks of carbonates at the end of the experiment were not significantly different among the treatments (Appendix D). However, the inorganic carbon sequestration potential could nonetheless be estimated based on significant changes in total alkalinity release estimated via the total amount of K, Mg and Ca recovered from plant, leachates and soil available pools compared to the unamended control (Table 4). Biochar addition did not significantly influence alkalinity release (Table 4). Basalt addition significantly increased total alkalinity release, whether applied alone or co-applied with biochar. P, K, Mg, Ca and total alkalinity release rates did not significantly differ between basalt alone and basalt and biochar co-applied (Appendix E, F). Alternative total alkalinity release rates estimates, based on isotopically estimated Ca release rates, similarly did not significantly differ between basalt alone and basalt and biochar co-applied (Appendix G). Modelling indicated no significant co-application effect of basalt and biochar on total alkalinity release, estimated via cation budget or corrected via isotopically estimated Ca release (Appendix H, I). Converted to C sequestration potentials, total alkalinity release rate for basalt alone resulted in a carbon sequestration potential of 1.13 ± 0.39 t of equivalent CO_2 ha^{-1} over the course of the experiment, extrapolated to 31.43 ± 9.89 kg of equivalent CO_2 t $rock^{-1}$ $year^{-1}$ (Table 5, Appendix J). Biochar and basalt co-applied resulted in 1.36 ± 0.30 t of equivalent CO_2 ha^{-1}, extrapolated to 38.12 ± 8.47 kg of equivalent CO_2 t $rock^{-1}$ $year^{-1}$ (Table 5, Appendix J).

3.2. Total soil carbon stocks

Basalt addition did not lead to detectable changes in soil total carbon stock compared to the unamended control (Table 5). Biochar addition, alone or co-applied with basalt, increased soil total carbon stocks compared to control by an average of 32 t of equivalent CO_2 ha^{-1} (Table 5). Total soil carbon stocks at the end of the experiment did not significantly differ between biochar alone or co-applied with basalt.

3.3. Soil-atmosphere greenhouse gas fluxes

The dynamics of soil CO_2, N_2O and CH_4 emissions over the course of the experiment did not reveal any significant effects of the treatments (Appendix K). Emission rates varied mainly as a function of the time elapsed since the start of the experiment and soil moisture during the measurements. Similarly, the cumulative GHG fluxes over the course of the experiment did not show any statistically significant effects (Appendix L).

3.4. Isotopic evidence for basalt dissolution

Initial soil $^{87}Sr/^{86}Sr$ isotopic ratio was 0.70893 ± 0.00004, biochar was 0.70863 ± 0.00004 and total basalt was 0.70356 ± 0.00001. At harvest, control soil average $^{87}Sr/^{86}Sr$ isotopic ratios were 0.70872 ± 0.00002 and 0.70884 ± 0.00010 for the topsoil and the bulk soil

Table 4
Total alkalinity flux and co-application effect.

Treatment	Total alkalinity (meq. $mesocosm^{-1}$)
CONT	0.00 ± 195.30^{a}
BIO	65.51 ± 191.18^{a}
BAS	607.55 ± 210.82^{b}
B + B	736.88 ± 163.78^{b}
ANOVA	$F_{3,21} = 8.12$, $P = 0.001$

For control (CONT), basalt (BAS), biochar (BIO) as well as the basalt and biochar co-application (B + B). Expressed as the difference from CONT. Different letters (a, b) indicate significant differences between treatments as determined by paired planned comparisons carried out on the raw fluxes. Error term represent ±1 SEM with uncertainty propagation from the 3 pools involved (soil, plant and leachates) and due to control mean subtraction.

Table 5
Inorganic carbon sequestration potential based on cation budget and change in total soil carbon stocks.

	Inorganic C sequestration potential (t CO_2 ha^{-1})	Δ Total soil C (t CO_2 ha^{-1})
CONT	0 ± 0.36[a]	0.00 ± 4.24[a]
BIO	0.12 ± 0.35[a]	33.38 ± 6.19[b]
BAS	1.13 ± 0.39[b]	3.94 ± 1.77[a]
B + B	1.36 ± 0.30[b]	31.25 ± 5.84[b]

Inorganic C sequestration potential assessed via alkalinity release during the experiment (approx. 6 months) with 0.75 mol CO_2 sequestration per mol alkalinity (Renforth, 2019). Changes in measured total soil C compared to the unamended control. For control (CONT), biochar (BIO), basalt (BAS) and basalt and biochar (B + B). Different letters (a, b) indicate significant differences between treatments as determined on total alkalinity release values before subtracting the control. For inorganic C sequestration potential, error term represent ±1 SEM after uncertainty propagation from the 3 pools involved (soil, plant and leachates) and due to control mean subtraction.

respectively, similar to initial soil (Fig. 2). Biochar addition did not significantly impact $^{87}Sr/^{86}Sr$ isotopic ratio in soil and plant (Fig. 2; See appendix M for full comparisons, for instance 0.70872 ± 0.00004 in topsoil after biochar addition). Basalt addition, alone or with biochar, resulted in a significant decrease in $^{87}Sr/^{86}Sr$ isotopic ratio in plant and soil (Fig. 2; See appendix M, for instance 0.70503 ± 0.00002 in topsoil after basalt addition and 0.70521 ± 0.00007 after basalt and biochar co-application).

$^{87}Sr/^{86}Sr$ ratios as a function of Sr:Ca ratios for potential Sr sources (initial soil, basalt and biochar) as well as in plant and soil (*i.e.* aboveground and exchangeable soil pool) for control (grey), basalt (red), biochar (blue) as well as the basalt and biochar co-application (green).

Based on $^{87}Sr/^{86}Sr$ isotopic ratio and assuming no fractionation between Ca and Sr during basalt dissolution (Capo et al., 1998), roughly 9.83 ± 0.22% Ca in plant and 21.85 ± 0.28%, 10.19 ± 0.83% Ca in soil pools (for the 0–100 and 100–300 mm soil layer respectively) were released from basalt dissolution for treatments amended with basalt alone. Basalt and biochar co-applied resulted in 10.01 ± 0.15% Ca in plant released from basalt and 19.26 ± 0.50%, 10.39 ± 0.75% Ca in soil released from basalt (for the 0–100 and 100-300-mm soil layer respectively, appendix N). Basalt alone or co-applied resulted in a similar percentage of Ca in plant and soil released from basalt in plant and in the 100–300 mm soil layer (Appendix N). In the topsoil (0–100 mm) the percentage of Ca in soil released from basalt was higher when basalt was applied alone than co-applied with biochar (P = 0.006) (Appendix N).

3.5. Plant biomass and nutrient uptake

Total wheat biomass did not significantly differ between the unamended mesocosms and those amended with either biochar or basalt alone, or with both biochar and basalt co-applied (Fig. 3). However, total biomass was higher for the mesocosms amended with both biochar

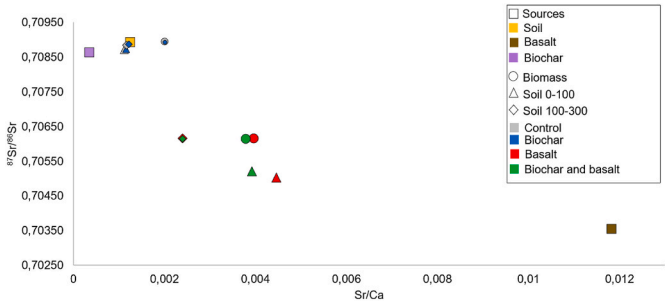

Fig. 2. Shifts in the strontium isotope composition of the major pools in the mesocosms as a function of their Sr:Ca ratio.

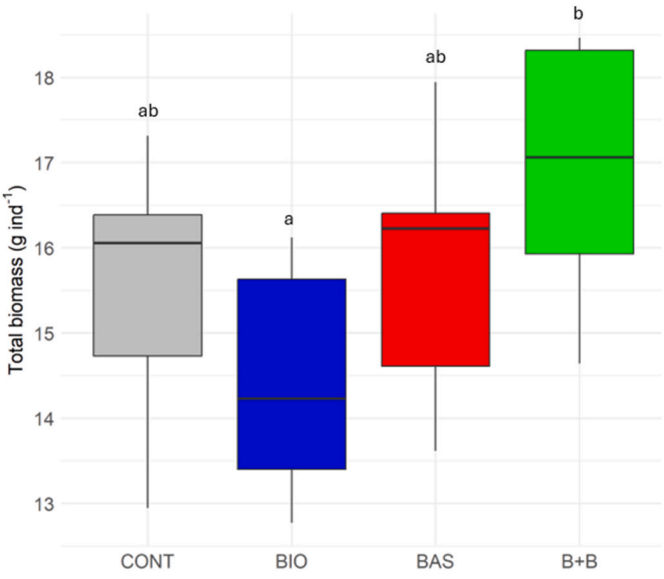

Fig. 3. Wheat biomass
Total plant biomass (g dry weight ind^{-1}) harvested in the control (CONT), basalt (BAS), biochar (BIO), and biochar and basalt amendments (B + B). Different letters (a, b) indicate significant differences between treatments. Error bars represent ±1 SEM.

and basalt co-applied than with biochar alone (Fig. 3) (refer to Appendix O for the detailed breakdown by plant organ, including roots, shoots, and seeds.)

Total nutrient plant uptake in mesocosms amended with basalt applied alone or biochar applied alone did not differ significantly from the unamended control (Fig. 4 1). Basalt and biochar co-applied nonetheless resulted in higher total plant K uptake than the unamended control (Fig. 4 1c) and higher total Mg uptake than biochar alone and than the unamended control (Fig. 4 1b). Plant total N uptake did not significantly differ between treatments (P = 0.113) (Appendix P).

3.6. Soil nutrient stocks and leaching

Biochar alone did not significantly affect P, K, Mg and Ca soil available pools measured at the end of the experiment (Fig. 4 2). Basalt addition significantly increased soil available P and Mg pools, by 43 and 109% respectively compared to the control (Fig. 4 2a, b). The effects of co-applying biochar and basalt were mostly not significantly different from those of basalt alone (Fig. 4 2). Basalt applied alone did not significantly increase soil available Ca compared to the control (Fig. 4 2). However, the availability of Ca in the soil was higher when biochar and basalt were co-applied compared to when biochar was applied alone, and also compared to the unamended control. The increase in Ca availability after basalt and biochar co-application was 126% of expected effects based on separate application. Increases in available nutrient pools were more pronounced in the topsoil and decreased with soil depth (Appendix Q).

Basalt and biochar alone or co-applied did not significantly influence soil total available nitrogen at the end of the experiment (based on $N–NO_3 + N–NH_4$) (P = 0.231) (Appendix R). Biochar alone increased pH by 0.2 (P = 0.032) compared to the control in the topsoil (Appendix S). Basalt addition, alone or with biochar, also increased soil pH by 0.7 and 0.8 (P < 0.001) compared to the control in the topsoil (Appendix S).

The experimental amendments did not significantly impact P, K, Mg and Ca total export in leachates during the experiment (Appendix T). Leachate pH similarly did not significantly differ between treatments (Appendix T).

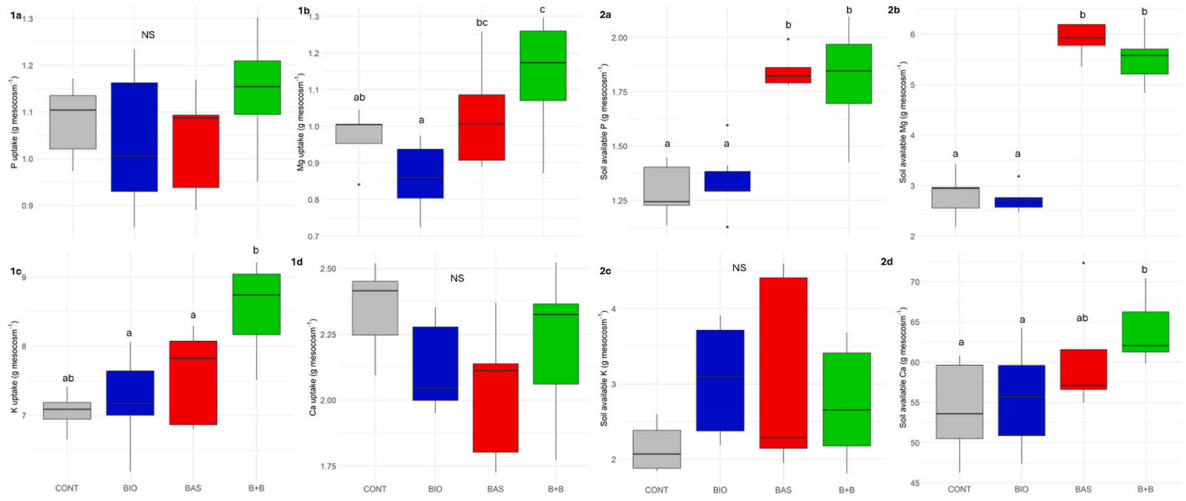

Fig. 4. Wheat P, K Mg and Ca uptake and cumulative mass of soil available nutrients per mesocosm.
Wheat total nutrient uptake (1) and available soil nutrient pools (2) for P (a), Mg (b), K(c) and Ca (d) in control (CONT), biochar (BIO), basalt (BAS) and basalt and biochar (B + B). Different letters above the bars represent statistically significant differences among treatments.

3.7. Ni and Cr accumulation and uptake

Ni concentration measured in wheat seeds increased compared to the unamended control after basalt addition alone (by 156%). Basalt and biochar co-applied also significantly increased seeds' Ni and Cr concentrations (by 79% and 74% respectively). Nonetheless, seed total Ni and Cr did not differ between basalt application alone and basalt co-applied with biochar (P = 0.421 and 0.613, Table 6).

4. Discussion

4.1. Co-application effects of basalt and biochar for carbon sequestration

Understanding synergies and complementarities between negative emission technologies is urgent in order to optimise their deployment and meet climate targets (Buss et al., 2021; Janssens et al., 2022; Hagens et al., 2023). Synergies in co-application of EW and biochar have been theorised based on complementary processes increasing silicate rock dissolution in the presence of biochar, and in turn alkalinity release (Amann and Hartmann, 2019). Based on total alkalinity release inorganic C sequestration potential in our experiment was 1.13 t of equivalent CO_2 ha^{-1} extrapolated (with $\eta = 1$ for comparison) to 42 kg of equivalent CO_2 t $rock^{-1}$ $year^{-1}$ for basalt alone and 1.36 t of equivalent CO_2 ha^{-1} extrapolated to 51 kg of equivalent CO_2 t $rock^{-1}$ $year^{-1}$ for basalt co-applied with biochar (Appendix J). Estimated carbon sequestration potentials are within the reported range for basalt application rates between 50 and 100 t ha^{-1} i.e., 24–73 kg of equivalent CO_2 t $rock^{-1}$ $year^{-1}$ (Kelland et al., 2020), 24–51 kg of equivalent CO_2 t $rock^{-1}$ $year^{-1}$ (Reershemius et al., 2023; Reynaert et al., 2023; Vienne et al., 2022) or 29–58 kg of equivalent CO_2 t $rock^{-1}$ $year^{-1}$ (Vienne et al., 2023). Co-application did not significantly affect total alkalinity release and thus total inorganic C sequestration potentials as highlighted by lack of significant interaction. High inherent uncertainty associated with proxies for alkalinity release likely contributed to this lack of difference (see part 4.4 for detailed discussion). Nonetheless, co-application effects tended to confirm consistent alkalinity release rates regardless of co-application, indicating nearly exactly additive effects. Total alkalinity release rate for basalt and biochar co-applied was 109% of their release when applied alone. Sr isotope analysis similarly indicated additive effects, with co-application resulting in 97 % of total alkalinity release rate when applied alone calculated based on isotopic estimates of Ca release rates. Moreover, isotopic evidence of basalt dissolution similarly overall indicated additive effects, with similar isotopic ratios achieved after addition of basalt and biochar co-applied and basalt alone.

The effects of biochar on soil properties, hypothesized to increase basalt dissolution (Amann and Hartmann, 2019; Azeem et al., 2022; Buss et al., 2021), were mostly indistinct from the unamended control in our experiment. Low responsiveness to biochar addition in our system likely contributed to our observations of overall additive effects. Nonetheless, our results provide first empirical evidence of additive rather than synergistic effects of basalt and biochar on basalt C sequestration potential. Our results underline that benefits of co-application of basalt and biochar may lie in complementary co-benefits for soil fertility and plant growth alongside unaltered basalt C sequestration potential.

Although the combined application of biochar and basalt has been proposed to yield synergistic effects on basalt dissolution and inorganic carbon sequestration, it is generally plausibly that the carbon sequestration capacity of biochar at least remains unaltered by its co-application with basalt (Amann and Hartmann, 2019; Buss et al., 2021). However, it has been suggested that concurrent increases in soil pH and nutrient availability when co-applied with basalt may increase biochar short term positive priming effect (Joseph et al., 2021) and thus reduce its overall C sequestration potential. In our experiment, no significant difference in CO_2 emissions were observed between amendments, as well as for emissions of other GHG such as N_2O and CH_4. Moreover, biochar applied alone or co-applied with basalt also resulted in similar total soil carbon pools, although fairly high variability was noted plausibly overshadowing treatment effects with an approx. 8% coefficient of variation (CV) on total soil carbon pools. Overall, similar stocks of total soil carbon at the end of the experiment and GHG emissions appear to support co-application of basalt and biochar without adverse on biochar C sequestration potential.

Table 6
Cr and Ni content in plant (mg kg^{-1}).

	Total Ni	Total Cr
CONT	1.6 ± 0.6^{a}	3.0 ± 1.0^{ab}
BIO	0.9 ± 0.2^{a}	1.6 ± 0.4^{a}
BAS	2.7 ± 0.3^{b}	4.8 ± 0.6^{bc}
B + B	2.9 ± 0.2^{b}	5.2 ± 0.5^{c}

Content for control (CONT), biochar (BIO), basalt (BAS) and basalt and biochar (B + B Seed total Ni: Total Ni concentration in seed; Seed total Cr: Total Cr concentration in seed. Different letters (a, b) indicate significant differences between treatments.

4.2. Co-benefit of basalt and biochar co-application for biomass, nutrient stocks and leaching

Beyond the suggested synergy for basalt inorganic carbon sequestration, co-application of biochar and basalt has been proposed to yield additional co-benefits for plant growth (Amann and Hartmann, 2019). Concurrent increases in soil pH, cation exchange capacity and nutrient availability, among others, have been conjectured to increase yields when co-applied (Amann and Hartmann, 2019; Buss et al., 2021; Smith, 2016). In our experiment, basalt and biochar applied alone did not affect wheat biomass, nutrient uptake or soil K and Ca availability (Fig. 3). Co-applied, basalt and biochar led to the highest biomass, albeit only significantly higher (by 7 % relative to the control) when compared to biochar alone. Wheat Mg and K uptake as well as soil P, Mg and Ca availability also improved for basalt and biochar co-applied compared to the unamended control. Effects seemed primarily driven by basalt addition, as biochar alone did not significantly affect wheat biomass, uptake and nutrient availability. Moderate biochar application rates of 12 t ha^{-1} (Joseph et al., 2021) of wood sourced ash poor biochar presumably contributed to relatively low biochar effects in our experiment (Dai et al., 2020; Major et al., 2010). While still scarce, evidence of basalt's effects on plant biomass ranges from no significant effects at 50 t basalt ha^{-1} on *Solanum tuberosum* yield to a 21% increase in *Sorghum bicolor* yield for 100 t basalt ha^{-1} (Kelland et al., 2020). Our results reinforce the low responsiveness of plant biomass observed for addition of 50 t basalt ha^{-1} (Vienne et al., 2022). However, the results confirm positive trends in plant K and Mg uptakes previously highlighted when adding 50 to 100 t ha^{-1} basalt (Kelland et al., 2020; Vienne et al., 2022) but only when co-applied with biochar. Enhanced weathering effects on plant nutrient uptake are often unclear, due to simultaneous increases in uptakes of multiple macro and micro nutrients (Reynaert et al., 2023). Nonetheless, co-application with biochar increased the uptake of nutrients released from basalt in our experiment, presumably through improved nutrient capture. This is supported by the specific root length data which showed an increased value for basalt and biochar co-applied compared to basalt alone in our experiment (Appendix U). Silicate EW has also been documented to lead to pronounced increases in Mg availability ranging from +100 to 700%, with +200–700% being observed for faster weathering rocks such as olivine (Amann et al., 2020; ten Berge et al., 2012). Our results of +109% Mg availability after basalt addition are within the expected range, and also indicate a 43% increase in P availability. In addition, an 18% increase in soil Ca availability was observed when co-applied with biochar, corresponding to a 126% increase in Ca availability compared to basalt and biochar effects alone.

4.3. Risk of basalt and biochar co-application

Basalt EW has been proposed as an alternative to faster weathering silicate minerals such as olivine due to reduced contents in potentially harmful trace elements (Beerling et al., 2018; Kantola et al., 2017). Biochar has moreover been extensively observed to reduce trace element availability and toxicity (Natasha et al., 2022). Perspectives for complementarities between basalt EW and biochar thus also include reduced side-effects of basalt co-applied with biochar due to sorption of harmful elements (Amann and Hartmann, 2019). Plant Ni and Cr concentrations did not significantly differ between basalt and biochar co-application and basalt application alone. Increased basalt dissolution when co-applied with biochar and low biochar effects might explain this lack of difference. The relatively lower content of Ni and Cr in the basalt used in this study (0.06% NiO and 0.09% Cr_2O_3) compared to other model rocks used in previous experiments (0.31% NiO in olivine, 0.37% NiO and 0.32% Cr_2O_3 in dunite for instance (ten Berge et al., 2012; Amann et al., 2020) may also have contributed to lower overall inputs. Lower addition of Ni and Cr may have been insufficient to detect plausible beneficial effects of biochar. However, increased plant Ni and Cr uptakes were indeed observed after basalt addition regardless of biochar co-application. Despite increased Ni uptake, wheat Ni content remained below threshold limits for phytotoxicity (ie. 5 mg kg^{-1}) (Poulik, 1997). Due to vastly varying phototoxicity per chemical speciation further assessing Cr plausible phytotoxicity would require additional measurements in addition to our total concentration (Kumar et al., 2016). Overall, we did not observe detectable benefits in terms of reduced uptake of EW-released Ni and Cr when co-applied with biochar. However, the comparatively low Ni and Cr content in basalt also contributed to lower inputs which plausibly lowered potential biochar benefits. This suggests that further investigations are warranted with silicate rocks more susceptible to these risks, such as olivine or dunite.

4.4. Caveats and limitations

Estimating C sequestration potential with short term experiments in real soil is a well-known challenge (Kelland et al., 2020; Reynaert et al., 2023; Vienne et al., 2022). Direct detection of changes in soil inorganic carbon accumulation have been suggested to require a minimum of five years (Vienne et al., 2022). We indeed observed no significant effect of amendments on total carbonates (Appendix D). However, indirect measurement such as cation fluxes in soil, plant and leachates can offer robust estimates of inorganic C sequestration potential. Moreover, measurements of soil exchangeable cations are crucial during system adjustment following basalt addition (Vienne et al., 2023). Nonetheless, use of soil exchangeable cations does not account for formation of secondary minerals or other pathways rendering cations unavailable, providing a minimal estimate only (Dietzen et al., 2018; Kelland et al., 2020; Reynaert et al., 2023; ten Berge et al., 2012). Cation fluxes are moreover often synonymous with high uncertainties, *i.e.*, documented variance coefficient ranging from 23% to 224% compared to 20–152% in our experiment (Reynaert et al., 2023; Vienne et al., 2023). This high variability may have partly overshadowed treatment effects in our experiment, although it remained within the expected range. In addition, the inclusion of plant cation budget in our estimated total alkalinity release rate could overestimate total alkalinity. Cation uptake by plants is indeed charge-balanced by proton release, neutralizing initial alkalinity release (Dietzen and Rosing, 2023; Haynes, 1990). Nonetheless re-release upon plant decomposition is expected, provided that the plant material remains on site (Dietzen and Rosing, 2023). Plant cation uptake is thus often included in estimates of C sequestration granted later release (Kelland et al., 2020; Reynaert et al., 2023). Moreover, while lower, our estimates of C sequestration excluding plant uptake supported similar conclusions in term of additivity between basalt and biochar addition (Appendix C). Finally, measurements of belowground CO_2 and N_2O emissions within the uncultivated area, despite being in very close vicinity to the plants, may have impacted the soil efflux due to reduced root biomass underneath the collar insertion and thus associated microbial activity. While our measurements may offer a first proxy to soil respiration and N_2O emissions, further efforts with adequate design are needed to evaluate mesocosms overall gaz exchanges.

5. Conclusion and perspectives

Overall, the results support hypotheses (1) to (3), as we found experimental evidence documenting the existence of additive effects of co-application of basalt and biochar on C sequestration, availability of soil nutrients and plant performance. Co-application of basalt and biochar in our sandy soil did not result in significant interactions and produced nearly exactly additive estimates of C sequestration potential. Co-benefits for wheat biomass, nutrient uptake and availability also mostly proved additive and dominated by effects of basalt addition. However, synergistic tendencies between amendments were also observed for wheat K and Mg uptake, as well as Ca availability. Ca availability for basalt and biochar co-applied was 126% of expected effects based on separate application. Contrary to hypothesis (4), biochar addition did not mitigate uptake of potentially harmful trace

elements released from basalt. Our study provides first experimental evidence supporting additive effects of biochar and basalt, although the diverse properties and application rates of biochar are known to produce a wide range of responses. This suggests the need for further research to strengthen our observations by examining varied amendment properties, application rates, and abiotic conditions.

Funding

This work was supported by University of Montpellier via the call "Appel à projets MUSE « Recherche 2021 »: tremplin ERC & accélérateur d'innovation" funded by the ANR-16-IDEX-0006 contract. The PACE platform is supported by LabEx CeMEB, an ANR « Investissements d'avenir » program (ANR-10-LABX-04-01).

CRediT authorship contribution statement

Nicolas Honvault: Writing – review & editing, Writing – original draft, Visualization, Validation, Project administration, Methodology, Investigation, Formal analysis. **Marie-Laure Tiouchichine:** Writing – review & editing, Resources, Project administration, Methodology. **Joana Sauze:** Writing – review & editing, Methodology, Formal analysis, Data curation. **Clément Piel:** Writing – review & editing, Methodology, Data curation. **Damien Landais:** Writing – review & editing, Resources, Methodology. **Sébastien Devidal:** Writing – review & editing, Methodology. **Emmanuel Gritti:** Writing – review & editing, Methodology. **Delphine Bosch:** Writing – review & editing, Writing – original draft, Visualization, Resources, Methodology, Formal analysis. **Alexandru Milcu:** Writing – review & editing, Writing – original draft, Visualization, Validation, Supervision, Resources, Project administration, Methodology, Investigation, Funding acquisition, Formal analysis, Data curation, Conceptualization.

Declaration of competing interest

The authors declare that they have no known competing financial interests or personal relationships that could have appeared to influence the work reported in this paper.

Data availability

Data will be made available on request.

Acknowledgements

The authors would like to thank R. Leclerc, B. Buatois, F. Fort as well as the whole "PACE platform" (PACE - CEFE, Montpellier, France) for their technical assistance and access to technical facilities. We are also grateful to the "Pole Chimie Balard" for their help in characterizing the basalt, H. P. Schmidt for providing the biochar and F. Desprez for providing the wheat seeds. We also thank the analytical platforms of the university of Montpellier, the Geoscience unit for their help with producing and handling isotopic data, as well as the hydroscience and AETE ISO-OSU OREME platform for their technical assistance. We thank S. Abiven and the team of CEREEP ecotron IDF for their advice and running analyses, as well as the whole Ecotron team for their help running the experiment. This study benefited from the CNRS resources allocated to the French ECOTRONS Research Infrastructure, from the Occitanie Region and FEDER investments as well as from the state allocation 'Investissement d'Avenir' AnaEEFrance ANR-11-INBS-0001.

Appendix A. Supplementary data

Supplementary data to this article can be found online at https://doi.org/10.1016/j.apgeochem.2024.106054.

References

AFNOR, 2012. Recueil de normes: qualité des sols 1996. AFNOR Tour Europe, Paris.

Almaraz, M., Bingham, N.L., Holzer, I.O., Geoghegan, E.K., Goertzen, H., Sohng, J., Houlton, B.Z., 2022. Methods for determining the CO2 removal capacity of enhanced weathering in agronomic settings. Front. Clim. 4, 970429 https://doi.org/10.3389/fclim.2022.970429.

Amann, T., Hartmann, J., 2019. Ideas and perspectives: synergies from co-deployment of negative emission technologies. Biogeosciences 16, 2949–2960. https://doi.org/10.5194/bg-16-2949-2019.

Amann, T., Hartmann, J., Struyf, E., de Oliveira Garcia, W., Fischer, E.K., Janssens, I., Meire, P., Schoelynck, J., 2020. Enhanced Weathering and related element fluxes – a cropland mesocosm approach. Biogeosciences 17, 103–119. https://doi.org/10.5194/bg-17-103-2020.

Anda, M., Shamshuddin, J., Fauziah, C.I., 2013. Increasing negative charge and nutrient contents of a highly weathered soil using basalt and rice husk to promote cocoa growth under field conditions. Soil Tillage Res. 132, 1–11. https://doi.org/10.1016/j.still.2013.04.005.

Azeem, M., Raza, S., Li, G., Smith, P., Zhu, Y.-G., 2022. Soil inorganic carbon sequestration through alkalinity regeneration using biologically induced weathering of rock powder and biochar. Soil Ecol. Lett. 4, 293–306. https://doi.org/10.1007/s42832-022-0136-4.

Beerling, D.J., Kantzas, E.P., Lomas, M.R., Wade, P., Renforth, P., Sarkar, B., Andrews, M. G., James, R.H., Pearce, C.R., Mecure, J.-F., Pollitt, H., Holden, P.B., Khanna, M., Koh, L., Quegan, S., Pidgeon, N.F., Hansen, J., Banwart, S.A., 2020. The potential for large-scale CO2 removal via rock weathering on croplands. Nature 242–248. https://doi.org/10.1038/s41586-020-2448-9.

Beerling, D.J., Leake, J.R., Long, S.P., Scholes, J.D., Ton, J., Nelson, P.N., Bird, M., Kantzas, E., Taylor, L.L., Sarkar, B., Kelland, M., DeLucia, E., Kantola, I., Müller, C., Rau, G., Hansen, J., 2018. Farming with crops and rocks to address global climate, food and soil security. Nat. Plants 4, 138–147. https://doi.org/10.1038/s41477-018-0108-y.

Bosch, D., Maury, R.C., El Azzouzi, M., Bollinger, C., Bellon, H., Verdoux, P., 2014. Lithospheric origin for neogene–quaternary middle atlas lavas (Morocco): clues from trace elements and Sr–Nd–Pb–Hf isotopes. Lithos 205, 247–265. https://doi.org/10.1016/j.lithos.2014.07.009.

Brunauer, S., Emmett, P.H., Teller, E., 1938. Adsorption of gases in multimolecular layers. J. Am. Chem. Soc. 60, 309–319. https://doi.org/10.1021/ja01269a023.

Buckingham, F.L., Henderson, G.M., Holdship, P., Renforth, P., 2022. Soil core study indicates limited CO2 removal by enhanced weathering in dry croplands in the UK. Appl. Geochem. 147, 105482 https://doi.org/10.1016/j.apgeochem.2022.105482.

Buss, W., Yeates, K., Rohling, E.J., Borevitz, J., 2021. Enhancing natural cycles in agro-ecosystems to boost plant carbon capture and soil storage. Oxford Open Climate Change 1, kgab006. https://doi.org/10.1093/oxfclm/kgab006.

Capo, R.C., Stewart, B.W., Chadwick, O.A., 1998. Strontium isotopes as tracers of ecosystem processes: theory and methods. Geoderma 82, 197–225. https://doi.org/10.1016/S0016-7061(97)00102-X.

Cipolla, G., Calabrese, S., Porporato, A., Noto, L.V., 2022. Effects of precipitation seasonality, irrigation, vegetation cycle and soil type on enhanced weathering – modeling of cropland case studies across four sites. Biogeosciences 19, 3877–3896. https://doi.org/10.5194/bg-19-3877-2022.

Dai, Y., Zheng, H., Jiang, Z., Xing, B., 2020. Combined effects of biochar properties and soil conditions on plant growth: a meta-analysis. Sci. Total Environ. 713, 136635 https://doi.org/10.1016/j.scitotenv.2020.136635.

Dietzen, C., Harrison, R., Michelsen-Correa, S., 2018. Effectiveness of enhanced mineral weathering as a carbon sequestration tool and alternative to agricultural lime: an incubation experiment. Int. J. Greenh. Gas Control 74, 251–258. https://doi.org/10.1016/j.ijggc.2018.05.007.

Dietzen, C., Rosing, M.T., 2023. Quantification of CO2 uptake by enhanced weathering of silicate minerals applied to acidic soils. Int. J. Greenh. Gas Control 125, 103872. https://doi.org/10.1016/j.ijggc.2023.103872.

Ding, Y., Liu, Y., Liu, S., Li, Z., Tan, X., Huang, X., Zeng, G., Zhou, L., Zheng, B., 2016. Biochar to improve soil fertility. A Rev. Agron. Sustain. Dev. 36, 36. https://doi.org/10.1007/s13593-016-0372-z.

Ghimire, B., Hulbert, S.H., Steber, C.M., Garland-Campbell, K., Sanguinet, K.A., 2020. Characterization of root traits for improvement of spring wheat in the Pacific Northwest. Agron. J. 112, 228–240. https://doi.org/10.1002/agj2.20040.

Gillman, G.P., Burkett, D.C., Coventry, R.J., 2002. Amending highly weathered soils with finely ground basalt rock. Appl. Geochem. 17, 987–1001. https://doi.org/10.1016/S0883-2927(02)00078-1.

Hagens, M., Hartmann, J., Vicca, S., Beerling, D.J., 2023. Editorial: enhanced weathering and synergistic combinations with other CDR methods. Front. Clim. 5, 1244396 https://doi.org/10.3389/fclim.2023.1244396.

Hartmann, J., West, A.J., Renforth, P., Köhler, P., De La Rocha, C.L., Wolf-Gladrow, D.A., Dürr, H.H., Scheffran, J., 2013. Enhanced chemical weathering as a geoengineering strategy to reduce atmospheric carbon dioxide, supply nutrients, and mitigate ocean acidification: enhanced weathering. Rev. Geophys. 51, 113–149. https://doi.org/10.1002/rog.20004.

Haynes, R.J., 1990. Active ion uptake and maintenance of cation-anion balance: a critical examination of their role in regulating rhizosphere pH. Plant Soil 126, 247–264. https://doi.org/10.1007/BF00012828.

Hoffland, E., Kuyper, T.W., Wallander, H., Plassard, C., Gorbushina, A.A., Haselwandter, K., Holmström, S., Landeweert, R., Lundström, U.S., Rosling, A., Sen, R., Smits, M.M., Van Hees, P.A., Van Breemen, N., 2004. The role of fungi in weathering. Front. Ecol. Environ. 2, 258–264. https://doi.org/10.1890/1540-9295(2004)002[0258:TROFIW]2.0.CO;2.

Hossain, M.K., Strezov, V., Chan, K.Y., Nelson, P.F., 2010. Agronomic properties of wastewater sludge biochar and bioavailability of metals in production of cherry tomato (Lycopersicon esculentum). Chemosphere 78, 1167–1171. https://doi.org/10.1016/j.chemosphere.2010.01.009.

Ipcc, 2022. Global warming of 1.5°C: IPCC special report on impacts of global warming of 1.5°C above pre-industrial levels in context of strengthening response to climate change. Sustainable Development, and Efforts to Eradicate Poverty, first ed. Cambridge University Press. https://doi.org/10.1017/9781009157940.

Janssens, I.A., Roobroeck, D., Sardans, J., Obersteiner, M., Peñuelas, J., Richter, A., Smith, P., Verbruggen, E., Vicca, S., 2022. Negative erosion and negative emissions: combining multiple land-based carbon dioxide removal techniques to rebuild fertile topsoils and enhance food production. Front. Clim. 4, 928403 https://doi.org/10.3389/fclim.2022.928403.

Jeffery, S., Verheijen, F.G.A., Van Der Velde, M., Bastos, A.C., 2011. A quantitative review of the effects of biochar application to soils on crop productivity using meta-analysis. Agric. Ecosyst. Environ. 144, 175–187. https://doi.org/10.1016/j.agee.2011.08.015.

Joseph, S., Cowie, A.L., Van Zwieten, L., Bolan, N., Budai, A., Buss, W., Cayuela, M.L., Graber, E.R., Ippolito, J.A., Kuzyakov, Y., Luo, Y., Ok, Y.S., Palansooriya, K.N., Shepherd, J., Stephens, S., Weng, Z., Han, Lehmann, J., 2021. How biochar works, and when it doesn't: a review of mechanisms controlling soil and plant responses to biochar. GCB Bioenergy 13, 1731–1764. https://doi.org/10.1111/gcbb.12885.

Kantola, I.B., Blanc-Betes, E., Masters, M.D., Chang, E., Marklein, A., Moore, C.E., Von Haden, A., Bernacchi, C.J., Wolf, A., Epihov, D.Z., Beerling, D.J., DeLucia, E.H., 2023. Improved net carbon budgets in the US Midwest through direct measured impacts of enhanced weathering. Global Change Biology gcb 16903. https://doi.org/10.1111/gcb.16903.

Kantola, I.B., Masters, M.D., Beerling, D.J., Long, S.P., DeLucia, E.H., 2017. Potential of global croplands and bioenergy crops for climate change mitigation through deployment for enhanced weathering. Biol. Lett. 13, 20160714 https://doi.org/10.1098/rsbl.2016.0714.

Kantzas, E.P., Val Martin, M., Lomas, M.R., Eufrasio, R.M., Renforth, P., Lewis, A.L., Taylor, L.L., Mecure, J.-F., Pollitt, H., Vercoulen, P.V., Vakilifard, N., Holden, P.B., Edwards, N.R., Koh, L., Pidgeon, N.F., Banwart, S.A., Beerling, D.J., 2022. Substantial carbon drawdown potential from enhanced rock weathering in the United Kingdom. Nat. Geosci. 15, 382–389. https://doi.org/10.1038/s41561-022-00925-2.

Kelland, M.E., Wade, P.W., Lewis, A.L., Taylor, L.L., Sarkar, B., Andrews, M.G., Lomas, M.R., Cotton, T.E.A., Kemp, S.J., James, R.H., Pearce, C.R., Hartley, S.E., Hodson, M.E., Leake, J.R., Banwart, S.A., Beerling, D.J., 2020. Increased yield and CO 2 sequestration potential with the C 4 cereal Sorghum bicolor cultivated in basaltic rock dust-amended agricultural soil. Global Change Biol. 26, 3658–3676. https://doi.org/10.1111/gcb.15089.

Kirchner, J., 2001. Data analysis toolkit #5: uncertainty analysis and error propagation. UC California Berkeley Seismological Laboratory. Retrieved from. http://seismo.berkeley.edu/~kirchner/eps_120/Toolkits/Toolkit_05.pdf.

Kumar, V., Suryakant, P., Kumar, S., Kumar, N., 2016. Effect of chromium toxicity on plants: a review. Agriways 4 (1), 107–120.

Laird, D.A., Fleming, P., Davis, D.D., Horton, R., Wang, B., Karlen, D.L., 2010. Impact of biochar amendments on the quality of a typical Midwestern agricultural soil. Geoderma 158, 443–449. https://doi.org/10.1016/j.geoderma.2010.05.013.

Lakanen, E., Erviö, R., 1971. A comparison of eight extractants for the determination of plant available micronutrients in soils. Acta Agric. Fenn. 223–232.

Larkin, C.S., Andrews, M.G., Pearce, C.R., Yeong, K.L., Beerling, D.J., Bellamy, J., Benedick, S., Freckleton, R.P., Goring-Harford, H., Sadekar, S., James, R.H., 2022. Quantification of CO2 removal in a large-scale enhanced weathering field trial on an oil palm plantation in Sabah, Malaysia. Front. Clim. 4, 959229 https://doi.org/10.3389/fclim.2022.959229.

Lehmann, Johannes, Abiven, S., Kleber, M., Pan, G., Singh, B.P., Sohi, S.P., Zimmerman, A.R., Lehmann, J., Joseph, S., 2015. Persistence of biochar in soil. Biochar Environ. Manag.: Sci., Technol. Implement. 2, 233–280.

Lu, S.-G., Sun, F.-F., Zong, Y.-T., 2014. Effect of rice husk biochar and coal fly ash on some physical properties of expansive clayey soil (Vertisol). Catena 114, 37–44. https://doi.org/10.1016/j.catena.2013.10.014.

Luyckx, M., Hausman, J.-F., Lutts, S., Guerriero, G., 2017. Silicon and plants: current knowledge and technological perspectives. Front. Plant Sci. 8 https://doi.org/10.3389/fpls.2017.00411.

Major, J., Rondon, M., Molina, D., Riha, S.J., Lehmann, J., 2010. Maize yield and nutrition during 4 years after biochar application to a Colombian savanna oxisol. Plant Soil 333, 117–128. https://doi.org/10.1007/s11104-010-0327-0.

Natasha, N., Shahid, M., Khalid, S., Bibi, I., Naeem, M.A., Niazi, N.K., Tack, F.M.G., Ippolito, J.A., Rinklebe, J., 2022. Influence of biochar on trace element uptake, toxicity and detoxification in plants and associated health risks: a critical review. Crit. Rev. Environ. Sci. Technol. 52, 2803–2843. https://doi.org/10.1080/10643389.2021.1894064.

Palandri, J.L., Kharaka, Y.K., 2004. A Compilation of Rate Parameters of Water-Mineral Interaction Kinetics for Application to Geochemical Modeling.

Palansooriya, K.N., Wong, J.T.F., Hashimoto, Y., Huang, L., Rinklebe, J., Chang, S.X., Bolan, N., Wang, H., Ok, Y.S., 2019. Response of microbial communities to biochar-amended soils: a critical review. Biochar 1, 3–22. https://doi.org/10.1007/s42773-019-00009-2.

Paustian, K., Lehmann, J., Ogle, S., Reay, D., Robertson, G.P., Smith, P., 2016. Climate-smart soils. Nature 532, 49–57. https://doi.org/10.1038/nature17174.

Poulik, Z., 1997. The danger of cumulation of nickel in cereals on contaminated soil. Agric. Ecosyst. Environ. 63 (1), 25–29. https://doi.org/10.1016/S0167-8809(96)01122-X.

Pokharel, P., Ma, Z., Chang, S.X., 2020. Biochar increases soil microbial biomass with changes in extra- and intracellular enzyme activities: a global meta-analysis. Biochar 2, 65–79. https://doi.org/10.1007/s42773-020-00039-1.

R Core Team, R., 2022. R: A Language and Environment for Statistical Computing. R Foundation for Statistical Computing Austria. URL:https://www.R-project.org/.

Reershemius, T., Kelland, M.E., Jordan, J.S., Davis, I.R., D'Ascanio, R., Kalderon-Asael, B., Asael, D., Epihov, D.Z., Beerling, D.J., Reinhard, C.T., Planavsky, N.J., 2023. A new soil-based approach for empirical monitoring of enhanced rock weathering rates. https://doi.org/10.48550/ARXIV.2302.05004.

Ren, H., Lv, C., Fernández-García, V., Huang, B., Yao, J., Ding, W., 2021. Biochar and PGPR amendments influence soil enzyme activities and nutrient concentrations in a eucalyptus seedling plantation. Biomass Conversion and Biorefinery 11, 1865–1874. https://doi.org/10.1007/s13399-019-00571-6.

Renforth, P., 2019. The negative emission potential of alkaline materials. Nat. Commun. 10, 1401. https://doi.org/10.1038/s41467-019-09475-5.

Renforth, P., Pogge von Strandmann, P.A.E., Henderson, G.M., 2015. The dissolution of olivine added to soil: implications for enhanced weathering. Appl. Geochem. 61, 109–118. https://doi.org/10.1016/j.apgeochem.2015.05.016.

Reynaert, S., Vienne, A., De Boeck, H.J., D'Hose, T., Janssens, I.A., Nijs, I., Portillo-Estrada, M., Verbruggen, E., Vicca, S., Poblador, S., 2023. Basalt addition improved climate change adaptation potential of young grassland monocultures under more persistent precipitation regimes (preprint). SSRN. https://doi.org/10.2139/ssrn.4409460.

Roy, J., Rineau, F., De Boeck, H.J., Nijs, I., Pütz, T., Abiven, S., Arnone, J.A., Barton, C.V. M., Beenaerts, N., Brüggemann, N., Dainese, M., Domisch, T., Eisenhauer, N., Garré, S., Gebler, A., Ghirardo, A., Jasoni, R.L., Kowalchuk, G., Landais, D., Larsen, S.H., Leemans, V., Le Galliard, J., Longdoz, B., Massol, F., Mikkelsen, T.N., Niedrist, G., Piel, C., Ravel, O., Sauze, J., Schmidt, A., Schnitzler, J., Teixeira, L.H., Tjoelker, M.G., Weisser, W.W., Winkler, B., Milcu, A., 2021. Ecotrons: powerful and versatile ecosystem analysers for ecology, agronomy and environmental science. Global Change Biol. 27, 1387–1407. https://doi.org/10.1111/gcb.15471.

Schuiling, R.D., Krijgsman, P., 2006. Enhanced weathering: an effective and cheap tool to sequester Co2. Climatic Change 74, 349–354. https://doi.org/10.1007/s10584-005-3485-y.

Smith, P., 2016. Soil carbon sequestration and biochar as negative emission technologies. Global Change Biol. 22, 1315–1324. https://doi.org/10.1111/gcb.13178.

Swoboda, P., Döring, T.F., Hamer, M., 2022. Remineralizing soils? The agricultural usage of silicate rock powders: a review. Sci. Total Environ. 807, 150976 https://doi.org/10.1016/j.scitotenv.2021.150976.

ten Berge, H.F.M., van der Meer, H.G., Steenhuizen, J.W., Goedhart, P.W., Knops, P., Verhagen, J., 2012. Olivine weathering in soil, and its effects on growth and nutrient uptake in ryegrass (Lolium perenne L.): a pot experiment. PLoS One 7, e42098. https://doi.org/10.1371/journal.pone.0042098.

Uroz, S., Calvaruso, C., Turpault, M.-P., Frey-Klett, P., 2009. Mineral weathering by bacteria: ecology, actors and mechanisms. Trends Microbiol. 17, 378–387. https://doi.org/10.1016/j.tim.2009.05.004.

Vicca, S., Goll, D.S., Hagens, M., Hartmann, J., Janssens, I.A., Neubeck, A., Peñuelas, J., Poblador, S., Rijnders, J., Sardans, J., Struyf, E., Swoboda, P., Groenigen, J.W., Vienne, A., Verbruggen, E., 2022. Is the climate change mitigation effect of enhanced silicate weathering governed by biological processes? Global Change Biol. 28, 711–726. https://doi.org/10.1111/gcb.15993.

Vienne, A., Frings, P., Poblador, S., Steinwidder, L., Rijnders, J., Schoelynck, J., Vindušková, O., Vicca, S., 2023. Soil carbon sequestration and the role of earthworms in an enhanced weathering mesocosm experiment (preprint). SSRN. https://doi.org/10.2139/ssrn.4449286.

Vienne, A., Poblador, S., Portillo-Estrada, M., Hartmann, J., Ijiehon, S., Wade, P., Vicca, S., 2022. Enhanced weathering using basalt rock powder: carbon sequestration, Co-benefits and risks in a mesocosm study with Solanum tuberosum. Front. Clim. 4, 869456 https://doi.org/10.3389/fclim.2022.869456.

Wang, J., Xiong, Z., Kuzyakov, Y., 2016. Biochar stability in soil: meta-analysis of decomposition and priming effects. GCB Bioenergy 8, 512–523. https://doi.org/10.1111/gcbb.12266.

Wang, Y., Xiao, X., Chen, B., 2018. Biochar impacts on soil silicon dissolution kinetics and their interaction mechanisms. Sci. Rep. 8, 8040. https://doi.org/10.1038/s41598-018-26396-3.

Wang, Y., Yin, R., Liu, R., 2014. Characterization of biochar from fast pyrolysis and its effect on chemical properties of the tea garden soil. J. Anal. Appl. Pyrol. 110, 375–381. https://doi.org/10.1016/j.jaap.2014.10.006.

Wei, B., Peng, Y., Lin, L., Zhang, D., Ma, L., Jiang, L., Li, Y., He, T., Wang, Z., 2023. Drivers of biochar-mediated improvement of soil water retention capacity based on soil texture: a meta-analysis. Geoderma 437, 116591. https://doi.org/10.1016/j.geoderma.2023.116591.

Woolf, D., Amonette, J.E., Street-Perrott, F.A., Lehmann, J., Joseph, S., 2010. Sustainable biochar to mitigate global climate change. Nat. Commun. 1, 56. https://doi.org/10.1038/ncomms1053.

Xiang, Y., Deng, Q., Duan, H., Guo, Y., 2017. Effects of biochar application on root traits: a meta-analysis. GCB bioenergy 9, 1563–1572. https://doi.org/10.1111/gcbb.12449.

Zamanian, K., Pustovoytov, K., Kuzyakov, Y., 2016. Pedogenic carbonates: forms and formation processes. Earth Sci. Rev. 157, 1–17. https://doi.org/10.1016/j.earscirev.2016.03.003.

Zhang, Y., Wang, J., Feng, Y., 2021. The effects of biochar addition on soil physicochemical properties: a review. Catena 202, 105284. https://doi.org/10.1016/j.catena.2021.105284.